Response of neutral atom emissions in the low-latitude and high-latitude magnetosheath direction to the magnetopause motion under extreme solar wind conditions

S. Taguchi[1]
Universities Space Research Association, NASA Goddard Space Flight Center, Greenbelt, Maryland, USA

M. R. Collier, T. E. Moore, and M.-C. Fok
NASA Goddard Space Flight Center, Greenbelt, Maryland, USA

H. J. Singer
Space Environment Center, National Oceanic and Atmospheric Administration, Boulder, Colorado, USA

Received 17 July 2003; revised 24 November 2003; accepted 12 December 2003; published 9 April 2004.

[1] On 11 April 2001 the high velocity and density of the solar wind and the strong southward interplanetary magnetic field moved the dayside magnetopause inside of geosynchronous orbit. The Low Energy Neutral Atom (LENA) imager on the Imager for Magnetopause-to-Aurora Global Exploration (IMAGE) spacecraft in the magnetosphere observed significant emission in the magnetosheath direction. The total neutral atom flux from the dayside region, ignoring the neutral solar wind flux directly from the Sun, shows a threefold enhancement, and each of the three increases is coincident with the occurrence of the magnetopause inside 6.6 R_E. Observations by LENA also show that emission in the direction of the low-latitude and high-latitude magnetosheath is modulated in such a manner that the sources shift earthward/sunward and equatorward/poleward in the low-latitude and high-latitude sheath, respectively. A model based on the distributions of the sheath flux and of the number density of the hydrogen exosphere explains these characteristics as a result of the motion of the magnetopause having an indentation at the cusp, suggesting a means for monitoring the cusp motion using IMAGE/LENA. *INDEX TERMS:* 2724 Magnetospheric Physics: Magnetopause, cusp, and boundary layers; 2728 Magnetospheric Physics: Magnetosheath; 2784 Magnetospheric Physics: Solar wind/magnetosphere interactions; 2740 Magnetospheric Physics: Magnetospheric configuration and dynamics; *KEYWORDS:* cusp, neutral atoms, magnetopause, magnetosheath, solar wind, extreme conditions

Citation: Taguchi, S., M. R. Collier, T. E. Moore, M.-C. Fok, and H. J. Singer (2004), Response of neutral atom emissions in the low-latitude and high-latitude magnetosheath direction to the magnetopause motion under extreme solar wind conditions, *J. Geophys. Res.*, *109*, A04208, doi:10.1029/2003JA010147.

1. Introduction

[2] Dynamic features of the magnetopause have been revealed by empirical models based on large in situ data sets of magnetopause crossings [e.g., *Roelof and Sibeck*, 1993; *Petrinec and Russell*, 1996]. While these types of models have successfully predicted the motion of the magnetopause near the equatorial plane even for extreme solar wind situations [*Shue et al.*, 1998], it is still unclear to what extent the validity of the models, which assume cylindrical symmetry around the aberrated Sun-Earth direction, can be extended to the *X-Z* meridian structure. In this meridian the magnetopause has a cusp indentation, and the characteristics of this indentation, in particular, the solar wind control of the location, need to be clarified for a full understanding of the dynamic features of the magnetopause.

[3] However, it is not easy to clarify these detailed characteristics based on in situ observations. The main reason is that the cusp is highly dynamic and associated with turbulence [*Dunlop et al.*, 2000]. Another reason is that reported dayside high-latitude boundary crossings, even sunward or antisunward of the cusp (not for the cusp indentation itself), are not enough for the evaluation of models for a broad range of solar wind conditions, even if there are models that can include a cusp indentation structure [e.g., *Sotirelis and Meng*, 1999]. A statistical study [*Boardsen et al.*, 2000] based on the Hawkeye magnetopause crossings antisunward of the cusp has modeled the dependence of the high-latitude magnetopause on solar wind parameters. The data come from a relatively small range of IMF B_z, and it is unclear if the solar wind dependence of the magnetopause shape on the IMF B_z

[1]On leave from Department of Information and Communication Engineering, University of Electro-Communications, Tokyo, Japan.

0148-0227/04/2003JA010147$09.00

can be extrapolated to a broad range of solar wind conditions, including the extreme cases.

[4] The Low Energy Neutral Atom (LENA) imager [*Moore et al.*, 2000] on the IMAGE spacecraft is capable of taking a whole image in the *X-Z* meridian every 2 min, when the spacecraft orbital plane is within 45° of that meridian. *Collier et al.* [2001a] showed that neutral particles detected by LENA in the magnetosphere include the result of solar wind ions charge exchanging with hydrogen exosphere in the magnetosheath flow. *Collier et al.* [2001b], *Moore et al.* [2003], and *Fok et al.* [2003] reported that LENA observed strong brightening in the direction of the low-latitude sheath for the 31 March 2001 coronal mass ejection (CME) event. In this study, using an event for which LENA observed significant emission in the magnetosheath direction, while at the same time GOES 8 observed multiple crossings of the magnetopause in a similar meridian, we test if LENA data reflect the magnetopause shape in the *X-Z* meridian and if the observed variations represent the effect of magnetopause motion. Results show that the LENA emission distributions, looking at a wide range of the dayside magnetosheath, reflect the cusp indentation in the magnetopause shape, and that temporal characteristics can be explained in terms of the magnetopause motion.

2. Solar Wind Conditions for the Magnetosphere Compression on 11 April 2001

[5] Figure 1 shows solar wind conditions for the event that we analyzed in this study. Figures 1a–1d are solar wind data obtained at the ACE spacecraft located about 220 R_E upstream of the Earth. The ram pressure in Figure 1c was calculated from the density (Figure 1a) and speed (Figure 1b) with assumption of 4% He^{++} particles. In Figure 1d, we plotted 64 s averages of IMF B_z data that were created from original 16 s averages so as to make comparison between the IMF and plasma data easier.

[6] At 1528 UT (right vertical line in Figures 1a–1d) ACE observed a sharp increase in the solar wind dynamic pressure. The corresponding positive sudden impulse (SI^+) in the ground magnetic field is clearly identified in Figure 1e, the H component of the SYM index [*Iyemori and Rao*, 1996]. As the start of SI^+ we took 1548 UT (right line in Figure 1e), i.e., the first increase of more than 5 nT min^{-1}. The time lag from ACE to the Earth is then estimated to be 20 (=1548–1528 UT) min. A similar time lag can be obtained for another SI^+ at 1519 UT (Figure 1e) if we relate this SI^+ to the ram pressure jump at 1459 UT (left line in Figure 1), which is the largest jump before the major jump. The 20 min time lag is shorter than the simple solar wind convection time ~36 min, which is calculated from the ACE X location of 220 R_E and solar wind speed of ~650 km s^{-1}. However, such a difference is not surprising when we consider that large timing uncertainties exist in the solar wind convection [*Collier et al.*, 1998]. The shorter lag is reasonable when we assume that the phase fronts are along the magnetic field. ACE is located at negative Y (=−9 R_E) and the IMF has positive B_x and negative B_y components (not shown).

[7] During the interval in Figure 1, solar wind ions with energies between 47 and 65 keV/e (obtained by the ACE Electron, Proton, and Alpha Monitor), which includes the 50 keV/e low limit for LENA ion admittance, have a very steady flux at ~2.4 × 10^6 counts s^{-1} cm^{-2} sr^{-1} MeV^{-1} (not shown). This suggests that if the energetic ions penetrating the collimator cause LENA variation, it would be a relatively constant effect. In other words, if the LENA response varies, it strongly suggests that the LENA response is not due to the energetic ions [*Collier et al.*, 2001a]. As has also been noted by *Collier et al.* [2001a], enhancements of solar EUV might affect the LENA response. Solar EUV measured by SOHO [*Judge et al.*, 1998] was very steady for this event (not shown), and such a possibility can be excluded if the LENA response is not steady.

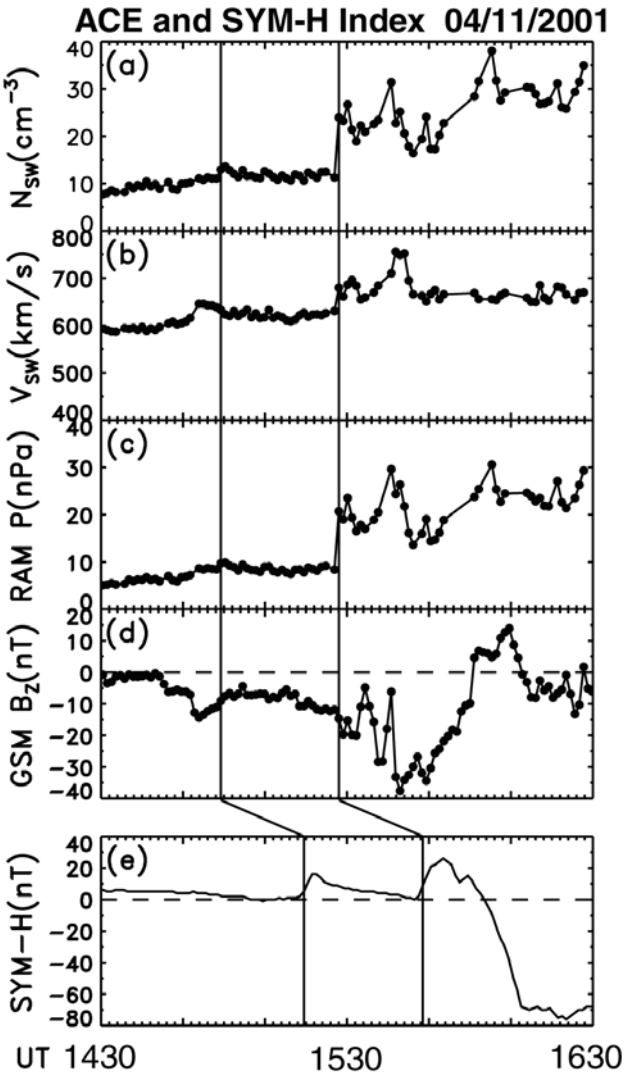

Figure 1. ACE solar wind data and SYM-H for the event in this study. The vertical lines in Figure 1e represent the times for the start of SI^+, and the times for the corresponding ACE ram pressure jump, which is identified in Figure 1c, are shown with the vertical lines Figures 1a–1d.

3. Variations of LENA Hydrogen Counts and GOES 8 Magnetic Field

[8] Figure 2 shows a LENA spectrogram for the same interval as Figure 1. The hydrogen count rates obtained by

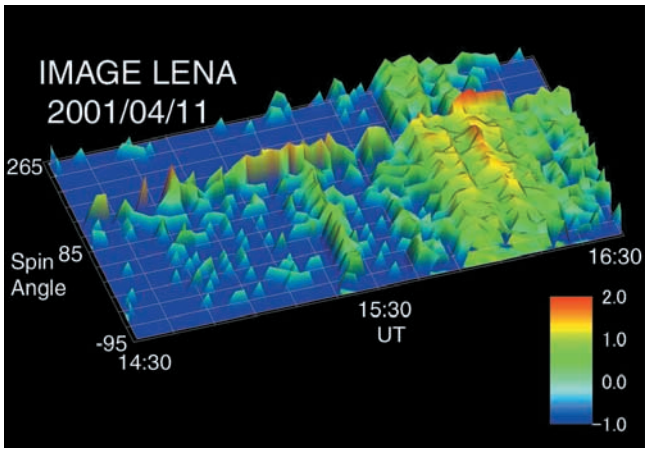

Figure 2. Low Energy Neutral Atom (LENA) spectrogram for the same interval as Figure 1. Background adjusted hydrogen count rates are plotted in spin angle versus UT. A strong emission started at ~1550 UT, and at 1524 UT a brief enhancement occurred. These two start times are very close to the start of the SI^+s in Figure 1.

summing up contributions over a whole energy range (10 to 300 eV) are plotted in the LENA spin angle versus UT. IMAGE was at $(X_{GSM}, Y_{GSM}, Z_{GSM}) = (3.8, 0.3, 6.1) \sim (4.1, -0.4, 3.4)$ during this interval. The line of sight (LOS) looking into the center of the Earth is included in an 8° spin angle bin from −7° to 1°, which is approximately the center of the −95° and 85° lines in Figure 2. The bright "undulating ridge," which starts near 115° in the spin angle axis and runs along the UT axis, represents neutral flux enhancements at the spin angle closest to the solar direction [*Moore et al.*, 2001; *Collier et al.*, 2001a, 2003].

[9] This "Sun signal" started to take large values around 1510 UT, and the high intensities continued until around 1530 UT. After that, the Sun signal sometimes showed relatively low intensities, and then started to increase again around 1550 UT. Approximately at 1605 UT the Sun signal took the maximum count during the interval of this plot. This sort of variability indicates that the Sun signal is not caused by energetic particle contamination because solar wind ions with energies between 47 and 65 keV/e from the ACE Proton, and Alpha Monitor show a very steady flux. As is described below in detail, strong emissions can be identified in a wide range of spin angle (not only at the Sun signal sector.) This also excludes the possibility of energetic particle contamination because energetic particles from the Sun are not expected to show such a wide range emission.

[10] A strong emission started at approximately 1550 UT. This occurs in a wide range of spin angles, i.e., the spin angles higher than the angle of the Sun signal as well as those looking in the region between the Earth and the Sun signal. It is also evident from Figure 2 that a brief enhancement occurs at 1524 UT before the major enhancement at 1550 UT. These two start times are very close to the start of the SI^+s at 1519 and 1548 UT. Since the SI^+ is caused by an increase of the solar wind dynamic pressure at the magnetopause, this close timing suggests that the hydrogen count enhancements identified by LENA can be related to the change of the solar wind density and/or velocity near the magnetopause, and/or the resultant magnetospheric phenomena such as the dayside magnetopause compression. The fact that SI^+ is earlier than the start of the emission enhancements has to be explained.

[11] Another possible association between the LENA emission and the solar wind can be seen in the comparison between the maximum count rates (except for the Sun signal) at 1603 UT and the corresponding solar wind. The solar wind during 1542–1544 UT, which is about 20 min before 1603 UT, had an extremely large negative value (approximately −35 nT) of the IMF B_z as well as a large ram pressure (Figure 1). After reaching this extreme value, the IMF B_z started to become less negative, and returned to about −20 nT around 1554 UT. This timing agrees with the reduction of the LENA emission seen around 1615 UT, when we consider the 20 min time lag. These facts show that a large negative B_z could be related to the LENA strong emission.

[12] A large negative B_z, as well as increasing of the dynamic pressure, is a controlling parameter for the reduction of the dayside magnetopause dimension [*Roelof and Sibeck*, 1993; *Petrinec and Russell*, 1996; *Shue et al.*, 1998, and references therein]. The above connection of the LENA emission to both the solar wind dynamic pressure and IMF B_z indicates that the reduction of the dayside magnetopause dimension is a major controlling parameter for the LENA emission enhancements. We give direct evidence to support this suggestion using the simultaneous GOES 8 observation below.

[13] Figure 3 shows the variations of the IMAGE position, the LENA spin angle ranges we used in our analysis, the LENA hydrogen total count rates, the normalized count profile versus spin angles, and the distance representing the direction for the maximum count peaks, together with the GOES 8 magnetic field (time resolution of ~0.5 s), the ACE solar wind, and the subsolar distance estimated from *Shue*'s [1998] model. The GOES 8 B_p component is parallel to the Earth's spin axis, and roughly in the GSM Z axis. The inset in Figure 3f shows the location of IMAGE and GOES 8 in the GSM X-Y plane between 1540 and 1620 UT. Both satellites were relatively closely located in the noon sector. GOES 8 was toward the noon meridian, and IMAGE was in a descending phase from apogee over the North Pole. B_p starts to increase about 1 min before 1548 UT, i.e., the time for the start of the major SI^+ on the ground, which is consistent with a rapid propagation of a compression wave launched at the dayside magnetopause by the shock front contact [e.g., *Araki*, 1994]. We then related the B_p increase at 1547 UT to the ACE ram pressure jump at 1528 UT, and plotted the 19 min shifted data in Figures 3g–3i.

[14] In Figure 3b, the spin angle sector that includes the Sun signal, which we have not focused on in this study, occurs between the two gray regions. The details of the cause of the Sun signal, including its long-term variations, has been reported by *Collier et al.* [2003, 2001a, 2001b]. IMAGE was located at positive Z, as shown in Figure 3a, and the spin angle range lower than the solar direction represents LOS that can intersect the equatorial plane. This lower angle range (lower shaded region in Figure 3b) for each time was determined as angles for which such intersection occurs between the radial distances of 4.5 R_E and of

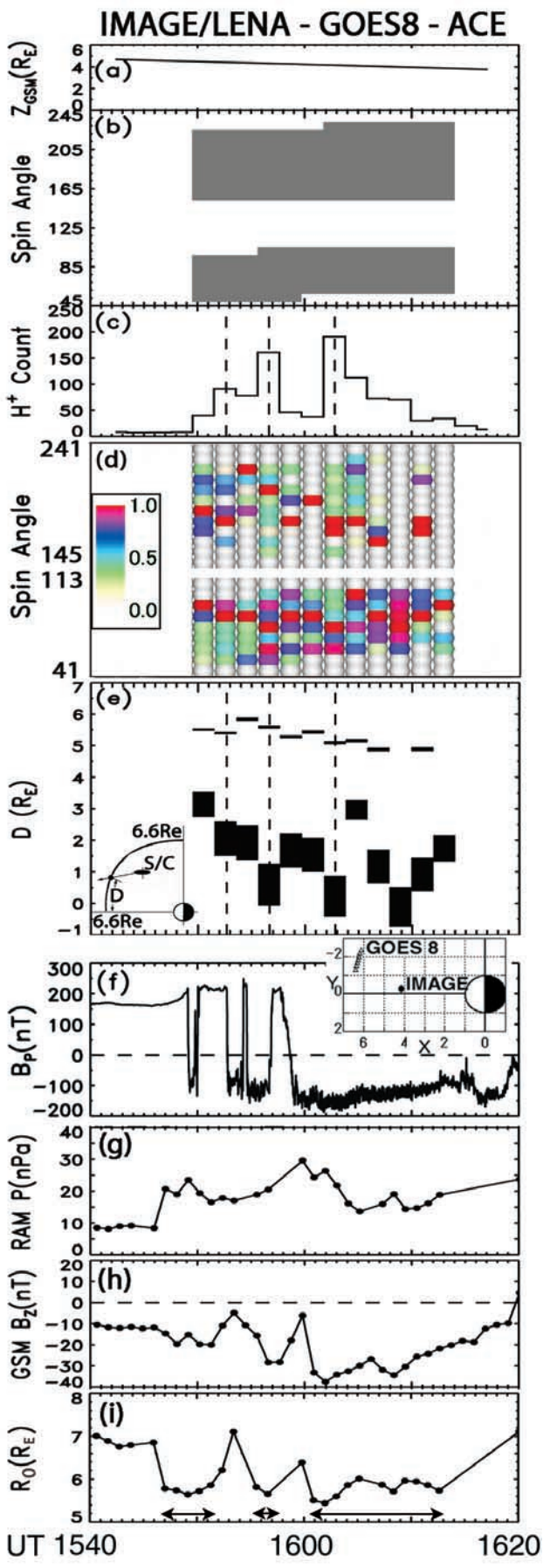

12 R_E, considering the possible subsolar distance of the magnetopause. For the higher shaded part, the lower boundary (157° bin) was taken as the sector that is three sectors (=24°) from the position of the Sun signal. The upper boundary was decided as a sector bin whose LOS makes the minimum angle from the Z axis.

[15] Figure 3c shows the total counts from the two gray regions. Three enhancements are identified around 1553, 1557, and 1603 UT (dashed lines). When we compare these LENA variations with the GOES 8 magnetic field data (Figure 3f), we find that each of these three enhancements occurs a few minutes after negative B_p initiates except for a very brief (~20 s) return to positive B_p at about 1554 UT. The negative B_p at GOES 8 can be interpreted as the spacecraft's exit into the magnetosheath from the magnetosphere after crossing the magnetopause. This agreement provides evidence for the response of the LENA variations to the magnetopause motion occurring in the vicinity of geosynchronous orbit with a timescale of several minutes.

[16] Figure 3d shows a spectrogram of the two gray regions in Figure 3b. Counts are normalized so that the maximum peak of the hydrogen background adjusted rate can be unity in each time and range. Blanks at 1609 and 1613 UT in the upper range mean that no emission is identified. In the upper range, emission peaks (red regions) shift to smaller angles in coincidence with the total count enhancements (in Figure 3c), which suggests that the source shifts equatorward at the enhancements. The emission in the lower range of Figure 3d shows similar variations of the peaks (red regions), and the two peaks at high and low latitudes tend to have correlative variations.

[17] This kind of characteristic can be more clearly identified for the locations of the peak count (Figure 3e). Figure 3e represents how distant the intersection of the LOS of the peak count; that is, the red dot (in Figure 3d) is from the equatorial plane as measured on the sphere of the radial distance of 6.6 R_E. The definition is illustrated in inset (Figure 3e). D = 0 means that the LOS intersects the equatorial plane at geosynchronous orbit. The wider D at low spin angle sectors simply represents that an 8° field of view is mapped to the more distant region while looking at the sphere with a smaller angle. There is a tendency that both peaks shift to a smaller or larger D region in a similar manner. The existence of this sort of correlative variation implies that these peaks have sources that originate from a common cause.

Figure 3. Variations of (a) the Imager for Magnetopause-to-Aurora Global Exploration (IMAGE) position, (b) the LENA spin angle, (c) the hydrogen total count rates, (d) the normalized counts in each time and range bin, (e) the distance representing the direction for the maximum count peaks, (f) the GOES 8 magnetic field, (g) the ACE dynamic pressure, (h) the magnetic field GSM Z component, and (i) the model subsolar distance during a period of the significant emission. The solar wind data and subsolar distance are shifted by 19 min. The inset of Figure 3e illustrates the definition of the distance D, which is plotted in this panel. The inset of Figure 3f shows the location of IMAGE and GOES 8.

[18] The variations of the subsolar distance obtained from *Shue*'s [1998] model using the data of ram pressure (Figure 3g) and IMF B_z (Figure 3h) are plotted in Figure 3i. We applied 64 s averages of solar wind input data to *Shue*'s [1998] model, although the model is based on 5 min averages of input data. Despite that higher time resolution input is used, the model result appears to represent the magnetopause motion identified by GOES 8. Three horizontal arrows in Figure 3i show the intervals during which R_0 is relatively small (less than approximately 6 R_E.) These roughly correspond to the intervals during which GOES 8 is outside the magnetopause, although the duration of each interval shown with the arrow does not agree exactly with the one during which GOES 8 is outside the magnetopause.

[19] The third interval during 1600–1613 UT appears to start when the IMF B_Z (Figure 3h) decreases rapidly by about 30 nT with the slight decrease of the ram pressure (Figure 3g). This suggests that the change of the IMF B_Z should be responsible for the reduction of the subsolar distance, and then for the LENA enhancement at the time of the third dashed line. This situation will be used later for modeling. For the first and second intervals in Figure 3i, however, it is difficult to determine unambiguously which solar wind parameter, IMF B_Z or ram pressure, is more closely related to the corresponding LENA enhancement, because at the start of each interval the ram pressure increases while the IMF B_Z decreases.

4. Modeling and Interpretation

[20] We show below that the shape of the dayside magnetopause in the *X*-*Z* meridian and the change of the shape and size can explain quasi quantitatively the characteristics of our observations. The neutral particle differential directional number flux J_{ENA} can be written as the integral of the intensity of ions, J_S multiplied by the charge exchange cross section σ and the neutral density N along the LOS [e.g., *Roelof and Skinner*, 2000]; that is,

$$J_{\mathrm{ENA}} = \int \sigma N J_S dL. \tag{1}$$

The intensity of ions at each point L along the LOS, $J_S(L)$ is the ion number flux per unit energy and unit steradian, and by defining the number flux per unit steradian as $F(L)_{\mathrm{LOS}}$, we can write the differential directional number flux integrated over energy, which is obtained by summing up contributions from the whole energy range of LENA, as follows:

$$\sum\nolimits_E J_{\mathrm{ENA}} (= I_{\mathrm{LENA}}) = \sigma \int N_{\mathrm{geo}}(L) F_{\mathrm{LOS}}(L) dL, \tag{2}$$

where we assume that σ is independent of energy because the variation of the cross section is very small, less than a factor of 1.5, for the reasonable collision energy range of the magnetosheath hydrogen that is considered below as the source. $N_{\mathrm{geo}}(L)$ represents the geocoronal density distribution.

[21] The source flux should have a maximum value F_{MAX} in the direction of the dominant vector of the sheath flow. Because such a direction is not necessarily along any LOS, the flux at a point along a given LOS is usually smaller than F_{MAX}. In other words, $F(L)_{\mathrm{LOS}} = F(L)_{\mathrm{MAX}} f(L)_{\mathrm{LOS}}$, where $f(L)_{\mathrm{LOS}} \leq 1$. To obtain a reasonable form of f_{LOS} we make a crude estimation based on a drift Maxwellian distribution. The phase space density along a line that makes an angle θ ($|\theta| \leq 90°$) from the vector of the drift flow V_{SH} has a peak at $V = V_{\mathrm{SH}} \cos\theta$, and the ratio of this peak relative to the peak in the direction of V_{SH} is exp $\{-(V_{\mathrm{SH}} \sin\theta/V_{\mathrm{T}})^2\}$, where V_T is the thermal velocity. Then the number flux along this line can be regarded as being reduced from $F(L)_{\mathrm{MAX}}$ by a factor of exp $\{-(V_{\mathrm{SH}} \sin\theta/V_{\mathrm{T}})^2\}\cos\theta$. This factor can be simplified as $\cos^{2K+1}\theta$, when we approximate $\exp(-\sin^2\theta)$ as $1 - \sin^2\theta$ by neglecting higher-order terms, and introduce K as the ratio of $(V_{\mathrm{SH}}/V_T)^2$.

[22] In general, V_{SH} increases with the downstream distance, and the situation is reversed for V_T [e.g., *Spreiter and Stahara*, 1985]. Thus the above ratio can differ greatly between the subsolar magnetosheath and the high-latitude magnetosheath. K could range from, for example, 9 for $V_{\mathrm{SH}} = 300$ km s^{-1} and $V_T = 100$ km s^{-1} to 0 for an extreme case for $V_{\mathrm{SH}} = 0$ that might be possible near the equatorial plane. A large value of K in $\cos^{2K+1}\theta$ as f_{LOS} means that significant $F(L)_{\mathrm{LOS}}$ is limited in a narrow direction almost parallel to V_{SH}. This means that the discrete emission in the high-latitude magnetosheath direction should represent the direction of the dominant sheath flow much better than the emission from the low-latitude sheath.

[23] In Figure 4 we show two magnetopause profiles (light blue and red curves) in which the sheath flow can have a dominant component toward the spacecraft location when the flow intrudes in the cusp indentation along the magnetopause. The spacecraft location is shown in $(X, Z) = (4.2, 4.2)$ R_E which is the actual position of the spacecraft around 1600 UT. We assumed that the flow intrusion occurs in the 197° bin (which covers 193°–201°) and 173° (169°–177°) of the LENA spin angle for the light blue-colored and red-colored magnetopause, respectively. These reflect situations at the time of the last enhancement (1603 UT in Figure 2) and just before the enhancement (1601 UT). As the distance of the cusp indentation, i.e., the distance of the equatorward edge of the cusp from the Earth, we chose 9 and 7 R_E. Although the selection of these distances makes the model reproduce the observed intensities well as is shown later, the determination of this distance is not the purpose of our modeling.

[24] The main purpose of our modeling is to show the possible profile of the neutral atom emissions created by the intrusion of the sheath flow to the cusp indentation. We do not attempt to reproduce the exact shape of the magnetopause near the cusp indentation. Besides the location of the equatorward edge of the cusp, we introduced several assumptions for the magnetopause shape so as to make calculation easier.

[25] The location of the poleward edge of the cusp is defined as being 1 R_E away from its equatorward edge in the direction that is perpendicular to the magnetopause. We took 15 R_E and 17 R_E as possible values for the magnetopause location at the Z axis from the average model obtained by *Boardsen et al.* [2000], somewhat reflecting an outward shift for the latter case with a larger southward IMF. The magnetopause between the point on the Z axis and the poleward edge of the cusp was modeled with a second-

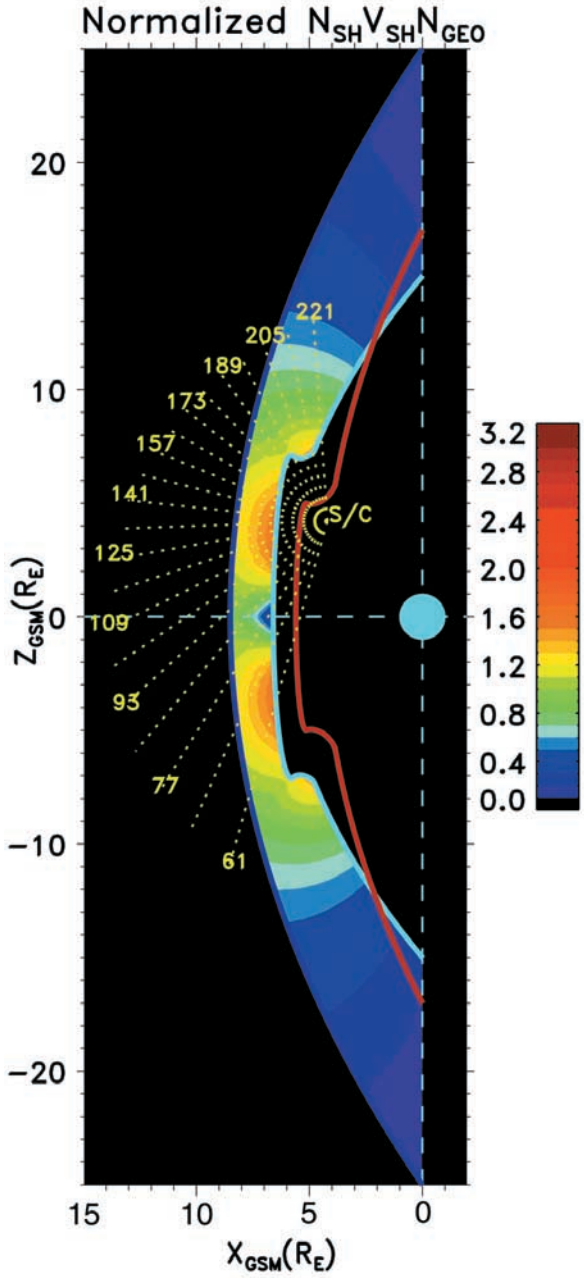

Figure 4. Distribution of the normalized neutral atom emission, i.e., the number flux multiplied by the geocoronal distribution factor $(1/R)^{2.91}$ in the modeled magnetosheath. Blue and red curves represent the two assumed magnetopause profiles. The dashed lines emerging from the point $(X, Z) = (4.2, 4.2)$ R_E represent the direction of each spin angle sector of LENA.

order polynomial function. As is shown later in our modeling, the shape of magnetopause on the tailward side of the cusp is not crucial as far as our purpose is concerned. The subsolar distance of the magnetopause was set to be 6.6 R_E for the light blue-colored magnetopause, and a further 1 R_E reduction was assumed for the red-colored one. These are based on the fact that GOES 8 crossed the magnetopause around 1559 UT, and on the results from *Shue*'s [1998] model. We used an ellipsoid form for the magnetopause between the subsolar point and the equatorward edge of the cusp.

[26] The location of the subsolar bow shock and the bow shock at the Z axis for the larger (light blue colored) magnetopause is assumed to be 8.5 R_E, which is approximately 1.3 times 6.6 R_E, and 25 R_E, which is 1.7 times 15 R_E, respectively. The latter dimension is in line with results from *Peredo et al.* [1995]. The shape between these two points is approximated with a second-order polynomial function. We used the location just inside the bow shock (blue color curve in Figure 4) for the larger magnetopause as a reference point as is shown below. The bow shock shape for the smaller (red-colored) magnetopause was made with the subsolar distance of 7.3 R_E (1.3 × 5.6 R_E) and the Z axis point of 28.3 R_E (1.7 × 17 R_E) in the same manner (not shown in Figure 4). The selection of the bow shock position appears not to be crucial as far as our purpose is concerned. The magnetosheath near the magnetopause is much more important because our interest is the charge exchange with the geocorona whose density decreases rapidly with the radial distance from the Earth.

[27] The color code in Figure 4 is the model distribution of the normalized neutral atom emission which is included in the integral of the following equation:

$$I_{\mathrm{LENA}} = \sigma \int N_{\mathrm{geo}} N_{\mathrm{SH}} V_{\mathrm{SH}} \cos^{2K+1} \theta dL. \tag{3}$$

We chose *Rairden et al.*'s [1986] result, i.e., N_{geo} that is proportional to $(1/R)^{2.91}$ as geocoronal model. For N_{SH} and V_{SH}, we adopted numerical distributions from the *Spreiter and Stahara* [1985] model (their Figure 10). Although this model does not have a cusp indentation, we created the distributions from their radial profiles for each 1° elevation angle, so that the density and velocity variations in the cusp indentation can be smooth. We then normalized the distribution of $(1/R)^{2.91} N_{\mathrm{SH}} V_{\mathrm{SH}}$ by the value just inside the bow shock at the equatorial plane, as was mentioned above.

[28] Near the equatorial plane, the distribution has a rather small value because of the low flux. In Spreiter's model the velocity is zero at the point just outside the subsolar magnetopause, and this can be identified in the distribution. As the position is away from the equatorial plane near the magnetopause boundary, the value of the normalized distribution of $(1/R)^{2.91} N_{\mathrm{SH}} V_{\mathrm{SH}}$ increases while the distance from the Earth does not change much, but finally the value becomes very small because of the large distance from the Earth.

[29] Using this distribution, we estimate the value of equation (3). We do not consider the absolute I_{LENA}, but discuss how this intensity varies versus the LOS direction. That the magnetosheath can be a source that produces an adequate absolute value of the intensity has been shown for an event in *Collier et al.* [2001a] and for the one in *Collier et al.* [2001b], and *Moore et al.* [2003]. The yellow dashed lines in Figure 4 show the LOS along which we evaluate the integral. For simplicity, we assumed that the dominant direction of the sheath flow is parallel to the tangential direction of the magnetopause at intersection of the line having the same elevation angle as the location of the flow in the sheath.

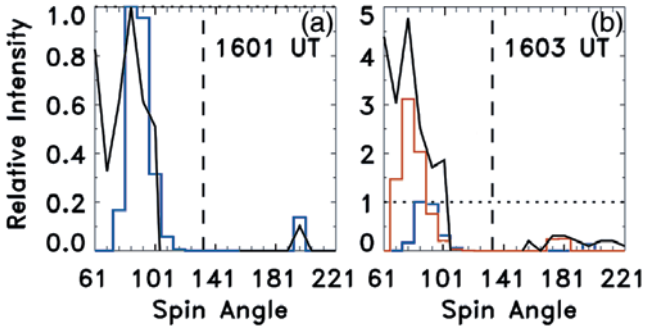

Figure 5. Modeling results of relative intensity of the sheath emission versus the spin angle and their comparison with the LENA hydrogen count rates. (a) An example for a larger magnetopause profile and (b) an example for a smaller profile. The blue and red lines represent the modeling results, and the LENA observation for comparison is indicated with the solid black lines. The vertical dashed line in each plot is the spin angle sector for the Sun signal.

[30] The blue line in Figure 5a shows the result from the integral of equation (3) for a case when K changes linearly from 0 at the equatorial sheath to 10 at the Z axis intersection with an increase of the elevation angle. The intensity is shown as a value relative to the maximum peak, which occurs at the spin angle of 85° (which looks into near the subsolar magnetopause). A minor peak can be identified at 197°, which corresponds to the cusp indentation, and the model shows a double peak structure. The black line represents hydrogen count rates measured in the sectors shown as the gray regions (Figure 3b) at 1601 UT. Data around the Sun signal (the vertical dashed lines) are not included in Figure 5. The measured count rates are also normalized by the maximum count rate, so that the intensity profile against the spin angle can be easily compared. It is evident that the double peak structure of the model can reproduce the general characteristics of the observation.

[31] Figure 5b represents how intensity is changed when the magnetopause profile becomes smaller (red curve in Figure 4). The blue line in Figure 5b is the same as the one in Figure 5a. It is clear that the peak originating in the low-latitude sheath moves to the left and increases by a factor of about 3, and that the peak from the cusp is also moved to the left with the emission range widening. This agrees with the characteristics of our observations at 1603 UT (black line).

[32] For Figure 5, we assumed that the distribution of the number flux profile in the sheath for the smaller magnetopause is the same as the one for the larger magnetopause, except that the former is situated closer to the Earth than the latter. This assumption is based on the fact that IMF B_z decreased rapidly by about 30 nT for the corresponding interval, and on the deduction that this IMF change affects the shape and size of the dayside magnetopause much more strongly than the change of the solar wind density and speed. For more detailed comparison between the observation and model, which is beyond the scope of this paper, temporal change of the flux distribution in the sheath should be considered.

[33] For both magnetopause profiles, the dominant contribution to the total count rate comes from the low-latitude sheath. The distance along the LOS of 85° is about 5 R_E. The neutral particles would take a few minutes to travel this distance from the source to the spacecraft because the speed of the neutral particles may be approximated as being the same the sheath flow speed, such as ~200 km s^{-1}. Compared with this few minutes travel time, the propagation time of hydromagnetic waves as SI^+ signals to the Earth from the dayside magnetopause is short, i.e., ~1 min [e.g., *Araki*, 1994]. The fact that SI^+ is earlier than the start of the emission enhancements is then reasonable.

5. Discussion and Conclusions

[34] We have shown that the LENA observations under an extreme solar wind condition can be interpreted as a result of the earthward/sunward motion of the magnetopause near the equatorial plane and the equatorward/poleward motion of the cusp where the sheath flow intrudes. This suggests that monitoring the magnetopause motion is possible with IMAGE/LENA. In particular, the possibility of monitoring the cusp would be important because the information of the cusp dynamics during extreme solar wind conditions is lacking when compared with the dynamics of the low-latitude magnetopause, which can be monitored constantly by many geosynchronous satellites. As has been mentioned in section 4, the discrete emission in the high-latitude sheath direction would represent the direction of the dominant sheath flow much better than the emission from the low-latitude sheath. This also means that monitoring the cusp with LENA is more significant.

[35] We suggest that two conditions are important for monitoring the cusp. One is that the solar wind compresses the magnetopause so that there is adequate charge exchange of the plasmas in the cusp with the hydrogen exosphere. Another condition concerns the spacecraft position. The spacecraft must be at lower latitudes than the cusp indentation and off the equatorial plane so that a wide separation can be acquired between the spin angle for the cusp and the one viewing the low-latitude magnetopause, and that the Sun signal may not overlap each of the two distributions.

[36] In the modeling we have adopted the flow distribution from the *Spreiter and Stahara* [1985] model in which the flow speed increases with the downstream distance, and assumed such a distribution even in the cusp. It would be interesting to consider how the flow and density profiles in the cusp are modified from the *Spreiter and Stahara* [1985] model. In reality, the sheath flow may slow down when it intrudes the cusp indentation. It should be noted that this possible slowdown is favorable for LENA's cusp monitoring because there is higher probability that the flow in the cusp will stay within nominal upper limit on energy for responding to converted negative ions.

[37] For the emission in the low-latitude sheath direction, while the location of the intersection of the LOS of the LENA low-latitude peak on the sphere of the radial distance of 6.6 R_E (lower plot of Figure 3e) shows variations that are generally in line with the GOES 8 observations (Figure 3f), the location on the sphere tends to be in a positive D, which means that the LOS of the peak count crosses the equatorial plane outside of 6.6 R_E even when the magnetopause is

inside 6.6 R_E. This tendency can be explained by our model (Figures 4 and 5a), in which the LOS of the peak intensity at the spin angle of 85° crosses the magnetopause at a positive Z_{GSM}. In Figure 4 it is the LOS of the spin angle 77°, which is the next to the sector for the peak count that passes through the point closest to the subsolar magnetopause.

[38] A large negative IMF B_z is associated with the strong sheath emission. Since the large negative B_z is also a key parameter for a storm, it is expected that strong sheath emission tends to occur in coincidence with a storm. In reality, the large negative B_z (approximately −35 nT) for the 11 April 2001 event which we analyzed in this study caused a storm. However, it should be noted that the storm state itself is not necessary for the significant sheath emission. When the strongest sheath emission occurred around 1603 UT on 11 April 2001, the SYM-H index was still positive (Figure 1), which means that the emission occurred before the storm developed. It is at the end of this day when *Dst* reached a minimum (−271 nT).

[39] These facts imply that monitoring the cusp with LENA is possible also for nonstorms if the solar wind dynamic pressure reduces the dayside magnetopause significantly without aid from southward IMF. A search for such nonstorm events would be done in the next step. Presumably, it will be easy considering the fact that some fraction of the emission around the Sun signal for the interval prior to CME arrival is due to charge exchange in the sheath [*Moore et al.*, 2001].

[40] In conclusion, using an event for which IMAGE/LENA observed significant emission in the magnetosheath direction, while at the same time GOES 8 observed multiple crossings of the magnetopause, we have shown that the LENA data reflect a magnetopause shape that has an indentation at the cusp. Also, variations in the LENA data represent the effect of the inward motion of the magnetopause near the equatorial plane and the equatorward motion of the cusp where the sheath flow intrudes. This study suggests that IMAGE/LENA can be a remote sensing tool for identifying the cusp motion, which is not easy to identify from in situ observations with a single spacecraft.

[41] **Acknowledgments.** S.T. wishes to thank D. Simpson for his conversation on the LENA spin angle geometry. ACE solar wind data are provided by NASA/NSSDC. The authors thank D. McComas (PI of ACE plasma data), N. Ness (PI of ACE magnetic field data), R. Gold (PI of ACE EPAM data), and D. Judge (PI of SOHO/SEM data). We also thank the WDC for Geomagnetism, Kyoto, Japan, for providing the midlatitude SYM-H index. This research was supported by the IMAGE Project under UPN 370-28-20 at Goddard Space Flight Center.

[42] Lou-Chuang Lee thanks the two reviewers for their assistance in evaluating this paper.

References

Araki, T. (1994), A physical model of the geomagnetic sudden commencement, in *Solar Wind Sources of Magnetospheric Ultra-Low-Frequency Waves*, *Geophys. Mongr. Ser.*, vol. 81, edited by M. Engebretson, K. Takahashi, and M. Scholer, pp. 182–201, AGU, Washington, D. C.

Boardsen, S. A., T. E. Eastman, T. Sotirelis, and J. L. Green (2000), An empirical model of the high-latitude magnetopause, *J. Geophys. Res.*, *105*, 23,193–23,219.

Collier, M. R., J. A. Slavin, R. P. Lepping, A. Szabo, and K. Ogilvie (1998), Timing accuracy for the simple planar propagation of magnetic field structures in the solar wind, *Geophys. Res. Lett.*, *25*, 2509–2512.

Collier, M. R., et al. (2001a), Observations of neutral atoms from the solar wind, *J. Geophys. Res.*, *106*, 24,893–24,906.

Collier, M. R., et al. (2001b), LENA observations on March 31, 2001: Magnetosheath remote sensing, *Eos Trans. AGU*, *82*(47), Fall Meet. Suppl., Abstract SM41C-05.

Collier, M. R., et al. (2003), Dust in the wind: The dust geometric cross section at 1 AU based on neutral solar wind observations, in *Solar Wind Ten*, edited by M. Velli, R. Bruno, and F. Malara, *AIP Conf. Proc.*, *679*, 790–793.

Dunlop, M. W., P. J. Cargill, T. J. Stubbs, and P. Woolliams (2000), The high-altitude cusps: HEOS 2, *J. Geophys. Res.*, *105*, 27,509–27,517.

Fok, M.-C., et al. (2003), Global ENA IMAGE simulations, *Space Sci. Rev.*, *109*, 77–103.

Iyemori, T., and D. R. K. Rao (1996), Decay of the *Dst* component of geomagnetic disturbance after substorm onset and its implication to storm substorm relation, *Ann. Geophys.*, *14*, 608–618.

Judge, D. L., et al. (1998), First solar EUV irradiances obtained from SOHO by the CELIAS/SEM, *Sol. Phys.*, *177*, 161–173.

Moore, T. E., et al. (2000), The low-energy neutral atom imager for IMAGE, *Space Sci. Rev.*, *91*, 155–195.

Moore, T. E., et al. (2001), Low energy neutral atoms in the magnetosphere, *Geophys. Res. Lett.*, *28*, 1143–1146.

Moore, T. E., M. R. Collier, M.-C. Fok, S. A. Fuselier, H. Khan, W. Lennartsson, D. G. Simpson, G. R. Wilson, and M. O. Chandler (2003), Heliosphere-geosphere interactions using low energy neutral atom imaging, *Space Sci. Rev.*, *109*, 351–371.

Peredo, M., J. A. Slavin, E. Mazur, and S. A. Curtis (1995), Three-dimensional position and shape of the bow shock and their variation with Alfvénic, sonic and magnetosonic Mach numbers and interplanetary magnetic field orientation, *J. Geophys. Res.*, *100*, 7907–7916.

Petrinec, S. M., and C. T. Russell (1996), Near-Earth magnetotail shape and size as determined from the magnetopause flaring angle, *J. Geophys. Res.*, *101*, 137–152.

Rairden, R. L., L. A. Frank, and J. D. Craven (1986), Geocoronal imaging with Dynamics Explorer, *J. Geophys. Res.*, *91*, 13,613–13,630.

Roelof, E. C., and D. G. Sibeck (1993), Magnetopause shape as a bivariate function of interplanetary magnetic field Bz and solar wind dynamic pressure, *J. Geophys. Res.*, *98*, 21,421–21,450.

Roelof, E. C., and A. J. Skinner (2000), Extraction of ion distributions from magnetospheric ENA and EUV images, *Space Sci. Rev.*, *91*, 437–459.

Shue, J.-H., et al. (1998), Magnetopause location under extreme solar wind conditions, *J. Geophys. Res.*, *103*, 17,691–17,700.

Sotirelis, T., and C.-I. Meng (1999), Magnetopause from pressure balance, *J. Geophys. Res.*, *104*, 6889–6898.

Spreiter, J. R., and S. S. Stahara (1985), Magnetohydrodynamic and gasdynamic theories for planetary bow waves, in *Collisionless Shocks in the Heliosphere: Reviews of Current Research*, *Geophys. Mongr. Ser.*, vol. 35, edited by R. G. Stone and B. T. Tsurutani, pp. 85–108, AGU, Washington, D. C.

M. R. Collier, M.-C. Fok, and T. E. Moore, NASA Goddard Space Flight Center, Code 692, Greenbelt, MD 20771, USA. (mcollier@pop600.gsfc.nasa.gov; mei-ching.fok@gsfc.nasa.gov; thomas.e.moore@gsfc.nasa.gov)

H. J. Singer, Space Environment Center, National Oceanic and Atmospheric Administration, 325 Broadway, Boulder, CO 80303, USA. (hsinger@sec.noaa.gov)

S. Taguchi, Department of Information and Communication Engineering, University of Electro-Communications, 1-5-1 Chofugaoka, Chofu, 182-8585 Tokyo, Japan. (taguchi@ice.uec.ac.jp)